scientific reports

OPEN

3D spectral CT-based fusion model predicts prognosis and postoperative adjuvant chemotherapy benefit in locally advanced rectal cancer

Shuxuan Fan[1,5], Jiaxin Liu[1,5], Xiaomeng Yang[1], Lisha Qi[2], Xiaomei Lu[3], Haiwei Liu[3] & Xiaonan Cui[1,4✉]

Early identification of high-risk recurrence patients is crucial as it can provide information for treatment decisions, achieve personalized treatment, and maximize the benefits for locally advanced rectal cancer (LARC). The goal of this study was to explore the impact of ROI selection on the repeatability of spectral detector CT (SDCT) imaging biomarkers and to investigate and visualize an interpretable multidimensional radiological-angiogenesis-clinicopathological integrated model (RACIM) for predicting disease-free survival (DFS) in LARC. 204 LARC patients who underwent SDCT scanning prior to any anticancer treatment were retrospectively included. Two observers independently measured the iodine concentrations and normalized iodine concentration (NIC) at venous/delayed phases (VP/DP) using two different ROI protocols (2D vs. 3D). Cox regression methods were applied to determine the independent risk predictors associated with DFS, which were used to develop a prediction model. Kaplan–Meier survival curves were used to explore the performance of RACIM for personalized risk stratification. The models' performance was assessed using the area under the receiver operating characteristic (ROC) curve (AUC). The SHapley Additive exPlanation (SHAP) algorithm was used to attribute interpretability to the optimal prediction model. The 3D-ROI method achieved satisfactory interobserver accuracy. Multivariate Cox regression analyses indicated that perineural invasion, CD105, histological grade and NICVP$_{3D}$ values were independent predictors of DFS. On this basis, a multidimensional RACIM was constructed and achieved AUCs of 0.95 and 0.93 in the training and validation cohorts, respectively. The RACIM-based classifier demonstrated good performance for discriminating patients at high and low risk of recurrence, and patients in the high-risk group were found to have a favorable response to postoperative adjuvant chemotherapy (P = 0.036). Moreover, SDCT-derived 3D quantitative biomarker displayed as the most important feature in SHAP, indicating the importance of quantitative radiological features in personalized risk stratification. This study laid the foundation for the large-scale standardized clinical application of SDCT in the future, and provided an optional novel approach for postoperative risk stratification and even chemotherapy beneficiaries selection in LARCs.

Keywords Spectral imaging, Rectal cancer, Angiogenesis, Risk stratification

Abbreviations

[1]Department of Radiology, Tianjin's Clinical Research Center for Cancer, State Key Laboratory of Druggability Evaluation and Systematic Translational Medicine, Tianjin Key Laboratory of Digestive Cancer, Tianjin Medical University Cancer Institute & Hospital, National Clinical Research Center for Cancer, Tianjin, China. [2]Department of Pathology, Tianjin's Clinical Research Center for Cancer, State Key Laboratory of Druggability Evaluation and Systematic Translational Medicine, Tianjin Key Laboratory of Digestive Cancer, Tianjin Medical University Cancer Institute & Hospital, National Clinical Research Center for Cancer, Tianjin, China. [3]CT Clinical Science, Philips Healthcare, Beijing, China. [4]Department of Radiology, Tianjin Medical University Cancer Institute & Hospital, Huanhuxi Road, Hexi District, Tianjin, China. [5]Shuxuan Fan and Jiaxin Liu contributed equally to this work. ✉email: cuixiaonan@tjmuch.com

DFS	Disease-free survival
DP	Delayed phase
IC	Iodine concentration
LARC	Locally advanced rectal cancer
LVI	Lymphovascular invasion
MVD	Microvessel density
NIC	Normalized iodine concentration
PNI	Perineural invasion
RACIM	Radiological-angiogenesis-clinicopathological integrated model
ROC	Receiver-operating characteristic
SDCT	Spectral detector CT
SHAP	SHapley Additive exPlanation
VEGF	Vascular endothelial growth factor
VN	Valentini's nomogram
VP	Venous phase

In the past decade, the development of total mesorectal excision and the widespread use of neoadjuvant chemoradiotherapy have significantly decreased the locoregional recurrence rate of locally advanced rectal cancer (LARC)[1–3] but 25–40% of LARC patients still experience systemic recurrence after surgery[4]. To reduce the incidence of systemic recurrence, the guidelines recommend postoperative adjuvant chemotherapy for LARCs with high-risk clinicopathological factors such as T4 tumor stage, poorly differentiated tumors, obstruction or perforation at the time of diagnosis, lymphovascular invasion (LVI), perineural invasion (PNI), positive margins, and fewer than 12 lymph nodes examined after surgery[5]. Valentini's nomogram (VN), which includes pathological stage, surgical procedure, and adjuvant chemotherapy status, was developed for prognostic prediction of LARC[6] and endorsed by the American Joint Committee on Cancer. However, its performance is still limited (local recurrence, c-index 0.68; distant metastasis, c-index 0.73)[7]. In addition, whether high-risk patients classified by these clinicopathological factors can benefit from adjuvant chemotherapy after surgery remains controversial[8,9]. At present, radiological imaging is widely used for early diagnosis and prognostic factor detection due to its advantages of being noninvasive, visible, dynamic, and comprehensive for evaluating tumor lesions. Tumor angiogenesis is also an important indicator for predicting patient prognosis[10–12]. Hence, integrating multidimensional information from clinical-imaging-angiogenesis data to construct a fusion prediction model might provide better performance for postoperative risk stratification and selection of chemotherapy benefit populations.

In fact, imaging evaluation relies on visual assessment by radiologists, and there may be low consistency in diagnostic results among radiologists, especially junior radiologists with limited experience. Spectral detector CT (SDCT) has become a popular research topic due to its ability to not only obtain anatomical information from conventional CT but also provide various quantitative parameter information based on material composition analysis[13]. However, the majority of studies based on SDCT have used 2D-ROI delineation at the maximum level of tumors[14–18]. Due to the heterogeneity of LARC and the uneven distribution of neovascularization in tumors, qualified imaging markers must be able to reveal information on all lesions and be stable. Therefore, early evaluation using reproducible 3D-SDCT imaging biomarkers may become an important parameter for improving prognostic prediction.

Angiogenesis is one of the core markers of cancer[19]. Multiple studies have shown that tumor angiogenesis, such as that of CD34 and CD105, and the level of vascular endothelial growth factor (VEGF) were important indicators for predicting patient prognosis[10–12] but the prognostic value of different angiogenesis parameters in RC remains controversial[20–22]. The identification of optimal angiogenesis biomarkers associated with the prognosis of LARC may provide additional prognostic value for the construction of prognostic models.

In this regard, we analyzed the impact of different ROI selection methods (2D vs. 3D) on the measurement of SDCT imaging biomarkers, explored the complementary prognostic value of different angiogenesis biomarkers, and established an interpretable model based on the optimal ROI protocol for individualized prediction of postoperative risk stratification in LARC patients. We further assessed and compared the prognostic value of our model to that of the VN model and tested its ability to determine the benefits of postoperative adjuvant chemotherapy in LARC patients.

Materials and methods
Patients
All studies complied with the Declaration of Helsinki. This retrospective study was approved by the institutional review boards of Tianjin Medical University Cancer Institute & Hospital (EK20240180), and patients informed consent was waived. All experiments were performed in accordance with relevant guidelines and regulations.

We retrospectively reviewed the data of rectal cancer patients who underwent pretreatment SDCT examination. Retrospective data between March 2019 and March 2021 were used to identify eligible patients according to the following inclusion criteria: (1) biopsy-proven untreated rectal cancer; (2) available pre-treatment pelvic SDCT images from the PACS; (3) standard neoadjuvant therapy followed by surgical resection with histopathological confirmation; and (4) no concurrent malignant tumors or prior cancer treatment. The exclusion criteria were as follows: (1) lost to follow-up within 3 years; or (2) had incomplete records of imaging, clinical and pathological data. The detailed information on preoperative treatment, surgery, and postoperative adjuvant therapy are shown in Supplementary Material 1.

Two rectal cancer cohorts were analyzed: 204 patients were randomly classified into training ($n = 143$) and validation ($n = 61$) cohorts at a 7:3 ratio, using the Python package scikit-learn, in Python 3.10.9. Figure 1 presents the flowchart for patient selection and the workflow of this study.

After surgical resection, all patients were followed up every 3–6 months for at least 3 years. The follow-up measurements included the CEA level and a contrast CT/MRI scan. The outcome of this study was 3-year disease-free survival (DFS), which was defined as the period between the date of surgery and the first evidence of clinical recurrence and/or distant metastases, as confirmed by imaging or histopathology. Patients were divided into recurrent and non-recurrent groups based on recurrence status within 3 years.

SDCT protocols and imaging feature acquisition

Rectal unenhanced and two-phase contrast-enhanced scans were performed by a dual-layer detector spectral CT (IQon Spectral CT, Philips Healthcare) in the supine position with hands above the head. First, under a tube voltage of 120 kVp, nonenhanced scanning was obtained following scout imaging. The nonionic contrast medium iohexol was applied as a contrast agent at a concentration of 1.2 mL/kg and an injection rate of 2.5 mL/s through the median cubital vein. The acquisition times in the venous phase (VP) and the delayed phase (DP) were 60–70 s and 90 s after contrast agent administration, respectively. The acquisition and reconstruction parameters are shown in Supplementary Material 2.

Spectral images were obtained on an IntelliSpace Portal Workstation (ISP version 10, Philips Healthcare) for further investigation. Two radiologists with abundant abdominal expertise (10 years and 12 years) and who were blinded to the clinical data, measured the quantitative imaging biomarkers independently. Two different ROI protocols were used. (1) For 2D-ROI, a round ROI was placed at the greatest axial diameter and adjacent to the upper and lower slices of the rectal cancer lesions, and then the average iodine concentration (IC) values on the iodine-based images were calculated (Fig. S1a,b,e,f). (2) For 3D-ROI, the volume of interest along the entire enhanced tumor margin at all visible tumor levels was outlined (Fig. S1c,d,g,h), and the average IC values were calculated. Additionally, the normalized iodine concentration (NIC) refers to the quotient of the lesion IC divided by the the same layer of external iliac artery IC to minimize patient variability (NIC = IClesion/ICartery).

Clinicopathological parameters

Clinicopathological parameters, including age, sex, hypertension history, family history, histologic grade, pathologic T, N stage, microsatellite instability status, HIF-1α expression, Ki-67 level, LVI, PNI, surgical procedure and postoperative adjunctive history, were collected by reviewing the medical records of the patients (Supplementary Material 3).

Tumor angiogenesis parameters

Tumor angiogenesis was assessed via the CD34-based microvessel density (MVD), CD105-based MVD, and VEGF level.

Immunohistochemistry was performed to stain selected specimens using monoclonal mouse anti-human CD34 and CD105 antibodies and monoclonal rabbit anti-human VEGF antibody (Supplementary Material 4,5).
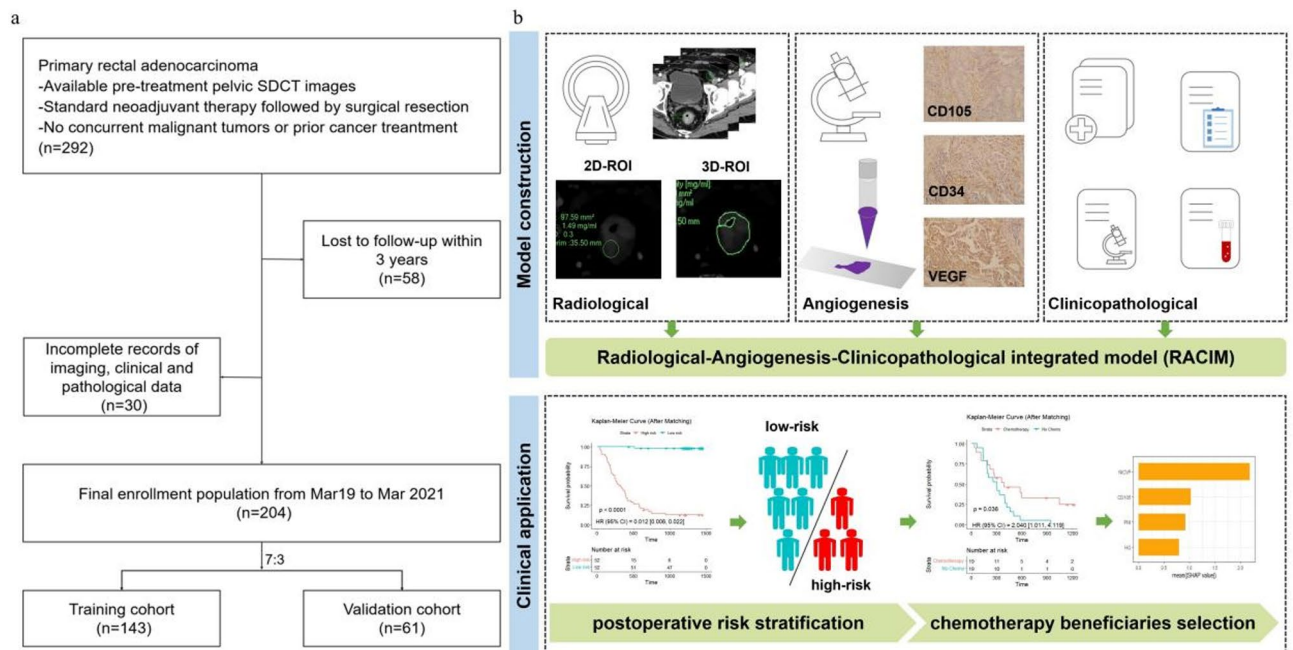

Fig. 1. Flowchart of patient's enrollment and the workflow of the study.

Model construction

The "xgboost" package in R was used to build the model, with the learning rate set to 0.1 and the objective function specified as binary logistic regression.

Statistical analyses

All the statistical calculations were conducted using SPSS 19.0, MedCalc 20.014 or R 6.1 (http://www.R-project.org). Quantitative variables are expressed as the mean ± SD. The data of the two observers were tested with the interclass correlation coefficient (ICC) and Bland-Ahman plot. Continuous variables were compared using the t-test or Mann-Whitney U tests, while categorical variables were compared using the χ^2 or Fisher exact tests, as appropriate. For continuous variables with missing values, use mean, median, or mode for imputation; For categorical variables, use mode interpolation. Cox proportional hazards model was used for univariate and multivariate analyses, effect sizes were reported as hazard ratios (HRs) with 95% confidence intervals (CIs). The DeLong test was adopted to compare the differences between parameters. The optimal cutoff value was determined using X-tile (3.6.1) for dividing patients into high-risk and low-risk groups. Patient stratification in different risk groups was evaluated using Kaplan–Meier curve analysis and the log-rank test. In order to control bias and achieve pseudo-randomization, propensity score matching (PSM) using R was used to rematch the study samples. To establish an interpretable prediction model, SHapley Additive exPlanation (SHAP) was used to provide an explanation for our predictive model, which calculated the importance of ranking features from the final model[23]. $P < 0.05$ was considered to indicate statistical significance.

Results

Patient characteristics

The baseline data of all 204 patients and their tumors are summarized in Table 1. The median follow-up times for DFS were 899.5 days in the training cohort (interquartile range [IQR]: 385.0–1257.0 days) and 950.4 days in the validation cohort (IQR: 499.0–1304.5 days).

Sixty-five of the 204 patients experienced disease recurrence, 33 (50.8%) of whom experienced systemic disease recurrence (8 in the lung, 20 in the liver, 2 in the bone and 3 in both the liver and lung), 21 (32.3%) of whom experienced locoregional disease recurrence, and 11 (16.9%) of whom experienced mixed disease. Among them, 20 patients were confirmed by surgery, while the other 45 patients were diagnosed based on radiological characteristics. 137 (67.2%) patients were treated with postoperative adjuvant fluorouracil-based chemotherapy.

Overall, the average CD34-based MVD of all the lesions was 40.19 ± 6.89; for CD105-based MVD, it was 28.25 ± 5.50.

2D- vs. 3D-ROI interobserver agreement

Among the two ROI methods, the 3D-ROI method had the best interobserver agreement (ICC of 0.826–0.960) (Table 2). The Bland-Altman analysis showed that all the imaging features measured by the 3D-ROI method were more concentrated than those measured by the 2D-ROI method, indicating that the 3D-ROI analysis had a smaller consistency interval and better accuracy in repeated measurements by different readers (Fig. 2). Therefore, the average values of 3D-quantitative imaging features calculated by the two radiologists were used for further analysis.

Predictive factors for DFS

In the univariate analyses of DFS, clinicopathological parameters (histologic grade, pT stage, pN stage, CEA, HIF-1α, LVI, and PNI), SDCT features (NICVP$_{3D}$ and NICDP$_{3D}$ values) and angiogenesis parameters (CD34, CD105, and VEGF) were associated with DFS. According to the multivariate analysis, clinicopathological parameters (PNI, histologic grade), SDCT features (NICVP$_{3D}$ values) and angiogenesis parameters (CD105) were found to be independent predictors in the training cohort ($P < 0.05$, Table 3).

Model construction and comparison

A multidimensional radiological-angiogenesis-clinicopathological integrated model (RACIM) was established based on the above prediction variables (PNI, CD105, histologic grade and NICVP$_{3D}$ values), which predicted the probability of disease recurrence for each individual patient. Multivariate analysis was used to construct a clinical model that included histologic grade, HIF-1α, LVI and PNI; an angiogenesis model that included CD105; and a radiological model that included NICVP$_{3D}$ values. The receiver-operating characteristic (ROC) curves of the different models for the entire cohort are shown in Fig. 3. The ROC curves revealed that the radiological model (NICVP$_{3D}$) had an AUC of 0.85 (95% CI, 0.78–0.91), a sensitivity of 78.4%, and a specificity of 79.3%. According to the X-tile, the optimal cut-off value of the NICVP$_{3D}$ was identified as 0.345. The combined model achieved excellent predictive performance, with AUCs of 0.95 (95% CI, 0.92–0.98) and 0.93 (95% CI, 0.85-1.00) in the training and validation cohorts, respectively (Table 4). The AUC of the combined model was obviously greater than that of the radiological ($P = 0.0004$, $P = 0.0393$), angiogenesis ($P < 0.0001$, $P = 0.0091$) and clinical models ($P = 0.0471$, $P = 0.0088$) in all cohorts.

Additionally, a VN model with pathological stage, surgical procedure, and adjuvant chemotherapy status was also built for comparison. Compared with the VN model (AUC: 0.77, 95% CI: 0.70–0.85; AUC: 0.76, 95% CI: 0.59–0.92; AUC: 0.72, 95% CI: 0.59–0.85), our radiological and RACIM models exhibited superior performance in the training (AUC: 0.85, 95% CI: 0.78–0.91, $P = 0.0160$; AUC: 0.95, 95% CI: 0.92–0.98, $P < 0.0001$) and validation (AUC: 0.83, 95% CI: 0.73–0.93, $P = 0.4217$; AUC: 0.93, 95% CI: 0.85-1.00, $P = 0.0428$) (Table 4). Moreover, the calibration plots of RACIM model showed that the estimations had good agreement with the

Characteristics	Training cohort ($n = 143$)	Validation cohort ($n = 61$)	P
Gender, n(%)			0.643
Male	77(53.8%)	35(57.4%)	
Female	66(46.2%)	26(42.6%)	
Age, n(%)			0.948
<60	64(44.8%)	27(44.3%)	
≥60	79(55.2%)	34(55.7%)	
HG, n(%)			0.958
Well	67(46.9%)	28(45.9%)	
Moderate	44(30.8%)	20(32.8%)	
Poor	32(22.4%)	13(21.3%)	
pT stage, n(%)			0.891
T1	19(13.3%)	10(16.4%)	
T2	27(18.9%)	13(21.3%)	
T3	39(27.3%)	15(24.6%)	
T4	58(40.6%)	23(37.7%)	
pN stage, n(%)			0.305
N0	83(58.0%)	42(68.9%)	
N1	42(29.4%)	12(19.7%)	
N2	18(12.6%)	7(11.5%)	
Smoking, n(%)			0.841
No	112(78.3%)	47(77.0%)	
Yes	31(21.7%)	14(23.0%)	
Hypertension, n(%)			0.722
No	102(71.3%)	42(68.9%)	
Yes	41(28.7%)	19(31.1%)	
Family history of cancer, n(%)			0.618
No	103(72.0%)	46(75.4%)	
Yes	40(28.0%)	15(24.6%)	
CEA, n(%)			0.418
Normal	90(62.9%)	42(68.9%)	
Abnormal	53(37.1%)	19(31.1%)	
CA242, n(%)			0.763
Normal	133(93.0%)	56(91.8%)	
Abnormal	10(7.0%)	5(8.2%)	
CA724, n(%)			0.992
Normal	129(90.2%)	55(90.2%)	
Abnormal	14(9.8%)	6(9.8%)	
CA199, n(%)			1.000
Normal	133(93.0%)	57(93.4%)	
Abnormal	10(7.0%)	4(6.6%)	
Ki-67 level, n(%)			0.158
Low	10(7.0%)	8(13.1%)	
High	133(93.0%)	53(86.9%)	
HIF-1α, n(%)			0.071
Low	60(42.0%)	34(55.7%)	
High	83(58.0%)	27(44.3%)	
MSI, n(%)			0.731
Low	111(77.6%)	46(75.4%)	
High	32(22.4%)	15(24.6%)	
VEGF, n(%)			0.289
Low	80(55.9%)	39(63.9%)	
High	63(44.1%)	22(36.1%)	
LVI, n(%)			0.847
Absent	106(74.1%)	46(75.4%)	
Present	37(25.9%)	15(24.6%)	
PNI, n(%)			0.349
Continued			

Characteristics	Training cohort ($n=143$)	Validation cohort ($n=61$)	P
Absent	122(85.3%)	55(90.2%)	
Present	21(14.7%)	6(9.8%)	
Recurrence, n(%)			0.258
No	92(64.3%)	47(77%)	
Yes	51(35.7%)	14(23.0%)	
Surgical procedure, n(%)			0.802
Low anterior resection	117(81.8%)	49(80.3%)	
Abdominoperineal resection	26(18.2%)	12(19.7%)	
Adjuvant chemotherapy, n(%)			0.505
No	47(32.9%)	23(37.7%)	
Yes	96(67.1%)	38(62.3%)	

Table 1. Clinicopathological parameters in all cohorts. HG = histologic grade; CEA = carcinoembryonic antigen; CA242 = carbohydrate antigen 242; CA724 = carbohydrate antigen 724; CA199 = carbohydrate antigen199; VEGF = vascular endothelial growth factor; MSI = microsatellite instability; LVI = lymphovascular invasion; PNI = perineural invasion; P values were calculated using the χ^2 or Fisher's exact tests.

	Interclass correlation coefficient			
	ROI-3D ($n=204$)		ROI-2D ($n=204$)	
	ICC	95%CI	ICC	95%CI
ICVP	0.874	0.838–0.903	0.683	0.603–0.750
ICDP	0.826	0.777–0.865	0.607	0.512–0.687
NICVP	0.960	0.947–0.969	0.767	0.704–0.818
NICDP	0.930	0.803–0.966	0.759	0.695–0.812

Table 2. The interclass correlation coefficient between the two observers using two different ROI methods. ICC = interclass correlation coefficient; IC = iodine concentration; NIC = normalized iodine concentration; VP = venous phase; DP = delayed phase.

actual observations (Fig. 4a,b). The decision curve analysis curves revealed that the RACIM model achieved moderately better net benefit than other models over the relevant threshold range in all cohorts (Fig. 4c, d).

Patient risk stratification

We divided patients into high- and low-risk groups according to the X-tile-generated optimum cutoff value (0.389) of the RACIM, which significantly differed in terms of DFS in the training cohort (log-rank test, $P < 0.001$) (Fig. 5a). Then, we performed the same analyses to stratify patients in the validation cohort to determine the prognostic value of the RACIM. Consistent with the training cohort, significant differences in DFS were observed between the two groups in validation cohort (log-rank test, $P = 0.001$) (Fig. 5b). Table 5 showed the selected prediction parameters in RACIM-classified high and low-risk groups.

To test the ability of the RACIM to identify patients who may benefit from postoperative adjuvant chemotherapy, subgroup analyses of patients receiving adjuvant chemotherapy were further performed. Notably, in the RACIM-classified high-risk group, postoperative adjuvant chemotherapy was significantly associated with a treatment benefit ($P = 0.036$), while adjuvant chemotherapy did not improve survival in any of the 204 patients ($P = 0.400$) or in patients with any high-risk clinicopathological features ($P = 0.400$, Fig. 6).

Model interpretability with SHAP

In this study, we employed the SHAP algorithm to endow our RACIM with global and local interpretability. As observed in the plot, the SDCT imaging indicator $NICVP_{3D}$ was the most important risk factor, followed by CD105, PNI, and histologic grade (Fig. 7a,b).

Figure 7c,d shows the SHAP model force plot of two male participants who had TNM stage IIIB disease, depicting how $NICVP_{3D}$, CD105 and clinicopathological characteristics affect the ability of the model to predict recurrence risk at the individual level.

Discussion

In this study, we first demonstrated that SDCT-derived 3D quantitative biomarkers achieved more satisfactory interobserver accuracy than 2D parameters and could reliably predict DFS in LARC patients. Compared to other angiogenesis parameters (CD34 and VEGF), CD105 was the only independent angiogenesis factor for DFS. We then developed and validated a multidimensional RACIM combining clinicopathological, SDCT and angiogenesis parameters (PNI, histologic grade, $NICVP_{3D}$, and CD105) for the individualized prediction of DFS and achieved better performance than traditional clinicopathological parameters. More importantly, the
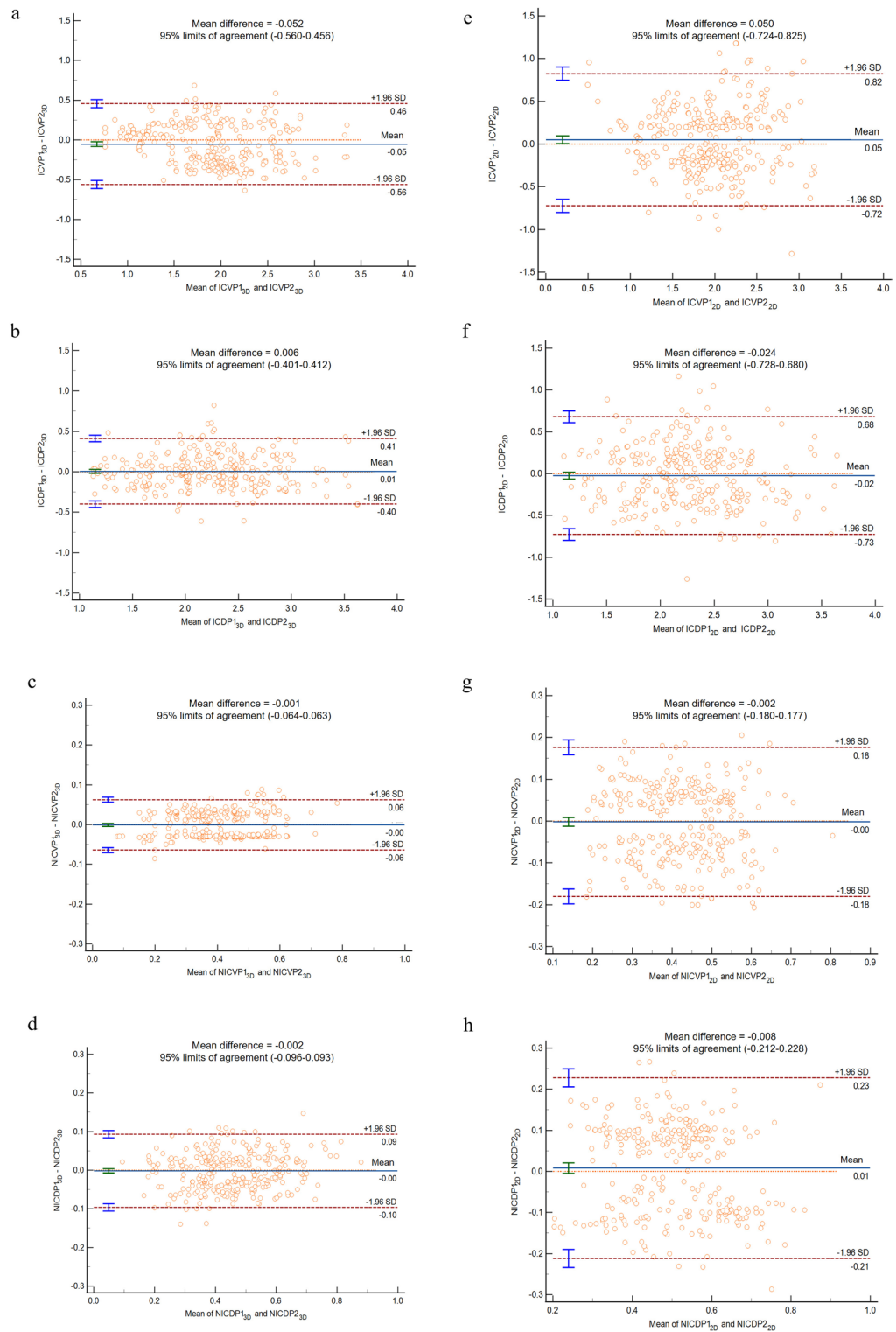
Fig. 2. Bland-Altman analysis between the two observers using two different ROI methods. (**a**) ICVP$_{3D}$. (**b**) ICDP$_{3D}$. (**c**) NICVP$_{3D}$. (**d**) NICDP$_{3D}$. (**e**) ICVP$_{2D}$. (**f**) ICVP$_{2D}$. (**g**) NICVP$_{2D}$. (**h**) NICDP$_{2D}$.

proposed RACIM successfully identified patients who were most likely to benefit from postoperative adjuvant therapy.

Over the past few years, many scholars have attempted to identify new biomarkers that can predict patient prognosis and help identify patients who are suitable for postoperative adjuvant chemotherapy in LARCs. Mounting evidence has revealed the predictive value of SDCT features in rectal cancer[14–18]. Previous studies selected only the maximum level of the tumor for ROI delineation, ignoring tumor heterogeneity and phenotypic

Variable	Univariate analysis HR (95%CI)	P Value	Multivariate analysis HR (95%CI)	P Value
HG		0.000*		0.041*
Well	Referent		Referent	
Moderate	1.843 (0.899–3.777)		1.459 (1.221–3.950)	
Poor	4.349 (2.205–8.575)		2.260 (1.516–5.079)	
pT stage		0.005*		0.439
T1	Referent		Referent	
T2	5.631 (0.693–45.780)		4.800 (0.475–48.461)	
T3	4.927 (0.858–50.763)		5.625 (0.604–52.370)	
T4	5.372 (1.901-102.188)		6.545 (0.677–63.330)	
pN stage		0.001*		0.074
N0	Referent		Referent	
N1	1.039 (0.532–2.031)		1.688 (0.215-2.200)	
N2	3.390 (1.725–6.663)		2.337 (0.704–7.759)	
CEA		0.001*		0.436
Normal	Referent		Referent	
Abnormal	2.669 (1.532–4.651)		1.460 (0.563–3.784)	
HIF-1α		0.002*		0.857
Low	Referent		Referent	
High	2.803 (1.466–5.358)		1.100 (0.391–3.094)	
VEGF		0.000*		0.492
Low	Referent		Referent	
High	2.836 (1.596–5.042)		1.458 (0.497–4.280)	
LVI		0.000*		0.068
Absent	Referent		Referent	
Present	3.834 (2.204–6.671)		2.520 (0.934–6.797)	
PNI		0.000*		0.002*
Absent	Referent		Referent	
Present	5.692 (3.182–10.179)		2.620 (1.753–5.179)	
CD34	1.132 (1.079–1.186)	0.000*	0.369 (0.121–1.126)	0.080
CD105	1.103 (1.049–1.158)	0.000*	1.258 (1.096–1.537)	0.006*
NICVP$_{3D}$	20.196 (5.269–77.412)	0.000*	19.475 (4.337–87.458)	0.000*
NICDP$_{3D}$	3.429 (1.211–9.704)	0.020*	0.703 (0.053–9.278)	0.789
Adjuvant chemotherapy		0.020*		0.697
No	Referent		Referent	
Yes	2.266 (1.135–4.526)		1.193 (0.491–2.902)	

Table 3. Univariate and multivariate logistic regression analysis for recurrence prediction in training cohort. HG = histologic grade; CEA = carcinoembryonic antigen; VEGF = vascular endothelial growth factor; MSI = microsatellite instability; LVI = lymphovascular invasion; PNI = perineural invasion; IC = iodine concentration; NIC = normalized iodine concentration; VP = venous phase; DP = delayed phase. *, $P < 0.05$. Significant values are in bold, $P < 0.05$.

variations. In contrast, our study showed that the 3D-ROI method has the best consistency and repeatability, thereby ensuring the reliability and stability of the results. In addition, our NICVP$_{3D}$ model was superior to any other parameter or VN model for predicting recurrence. Through the variance importance plot of the SHAP algorithm, we found that NICVP$_{3D}$ is also the most important feature, confirming the necessity of incorporating imaging features into conventional clinical features for risk stratification and laying the foundation for the large-scale standardized clinical application of SDCT in the future.

Notably, in our study, the NIC was an independent factor for DFS compared to the IC, and the venous-phase NIC outperformed the delay-phase NIC in terms of prognosis, which is consistent with the results of other studies[24–27]. The reason for these results may be that the NIC removed the potential influence of individual circulation on the IC, as well as the differences in tumor blood supply during different phases of contrast-enhanced CT. The iodine quantitative imaging biomarkers in the VP could well reflect the microcirculation of tumors and may reflect the distribution of contrast agents in the interstitial space[25,27]. However, other studies have also reported the predictive value of IC and NICDP in rectal cancer[26]. We speculated that this difference in the results may be attributable to the use of different ROI selection methods, although further investigations are needed before widespread implementation of these methods in clinical practice.
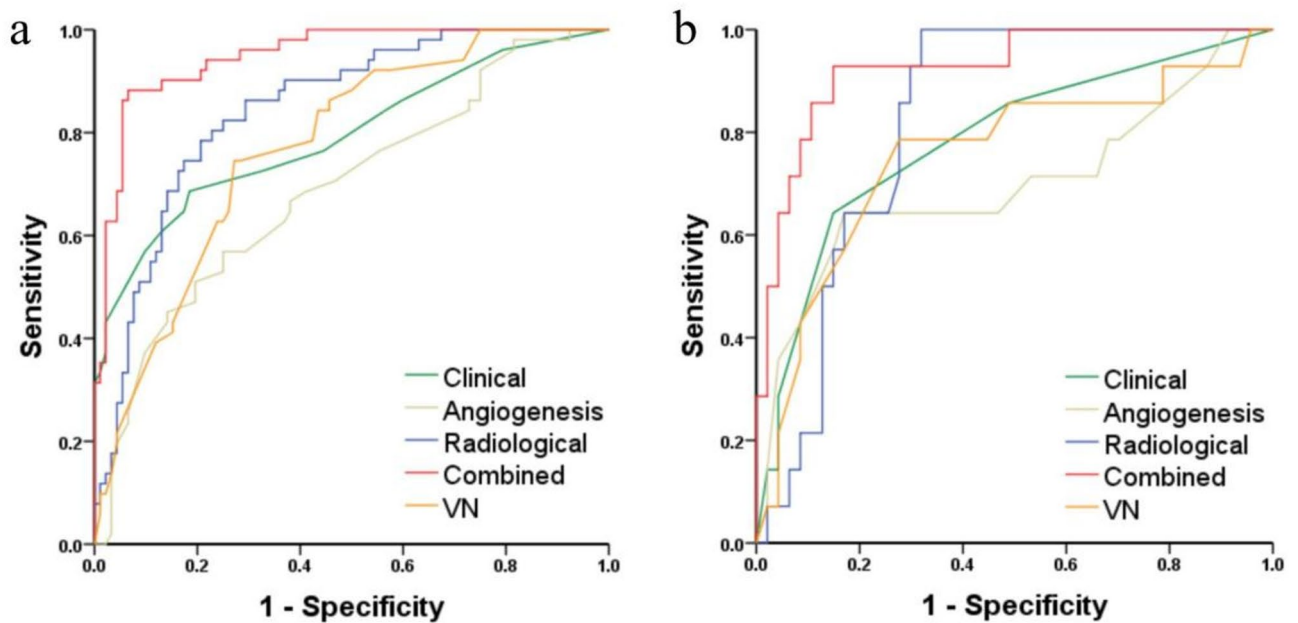
Fig. 3. Receiver operating characteristic curve (ROC) analysis for the prediction models in the training (**a**) and validation cohorts (**b**).

	Training cohort (n = 143)		Validation cohort (n = 61)	
	AUC	95%CI	AUC	95%CI
Clinical	0.79	0.71–0.88	0.78	0.64–0.93
Angiogenesis	0.69	0.60–0.78	0.70	0.52–0.89
Radiological	0.85	0.78–0.91	0.83	0.73–0.93
Combined	0.95	0.92–0.98	0.93	0.85-1.00
VN	0.77	0.70–0.85	0.76	0.59–0.92

Table 4. ROC analyses of the different models in the training and validation cohorts. CI = confidence interval; VN = Valentini's nomogram.

Angiogenesis is an important component of tumor progression; thus, our study incorporated angiogenesis parameters into the constructed predictive model. Notably, compared to VEGF and CD34, CD105-based MVD was the only independent factor for DFS, confirming that CD105 can be regarded as a better prognostic marker for rectal cancer, which is similar to the findings of a previous study[28]. CD105, a 180 kDa transmembrane glycoprotein, is a coreceptor of TGF-β and is the key factor in the TGF-β pathway and angiogenesis[29,30]. In contrast to CD31, CD34 and factor-related antigens, CD105 is highly expressed only in neovascular endothelial cells, while it is almost undetectable in the blood vessels of normal tissues[31]. Therefore, it is reasonable to explain why the average value of CD105-based MVD was lower than that of CD34-based MVD in the present study.

Another focus of this study was the selection of patients who benefited from adjuvant chemotherapy after surgery. According to our subgroup analyses, we found that patients in the RACIM-based high-risk group achieved a better survival benefit from adjuvant chemotherapy, whereas patients in the low-risk group did not. Furthermore, this study revealed that adjuvant chemotherapy failed to significantly improve survival outcomes in either the overall patient cohort or subgroups stratified by conventional high-risk clinicopathological parameters. These findings reaffirm the inherent limitations of traditional clinicopathological risk assessment in identifying optimal candidates for postoperative chemotherapy. Importantly, our novel RACIM-based classifier demonstrated superior predictive capacity for therapeutic stratification, enabling more personalized adjuvant treatment decisions through precision patient selection.

As a preliminary effort, the study has a few limitations. First, as a retrospective study, it was characterized by unavoidable selection bias. Second, the data were based on small numbers of patients from one center and lacked external validation. For this reason, future studies with more samples are needed to verify the model, and integrated research with antiangiogenic agents and neoadjuvant therapies are promising future directions. Finally, manual segmentation was time-consuming. To our knowledge, the IntelliSpace Portal workstation 12 has achieved semiautomatic volumetric ROI delineation, which will provide convenient technical support for further validation of our results.
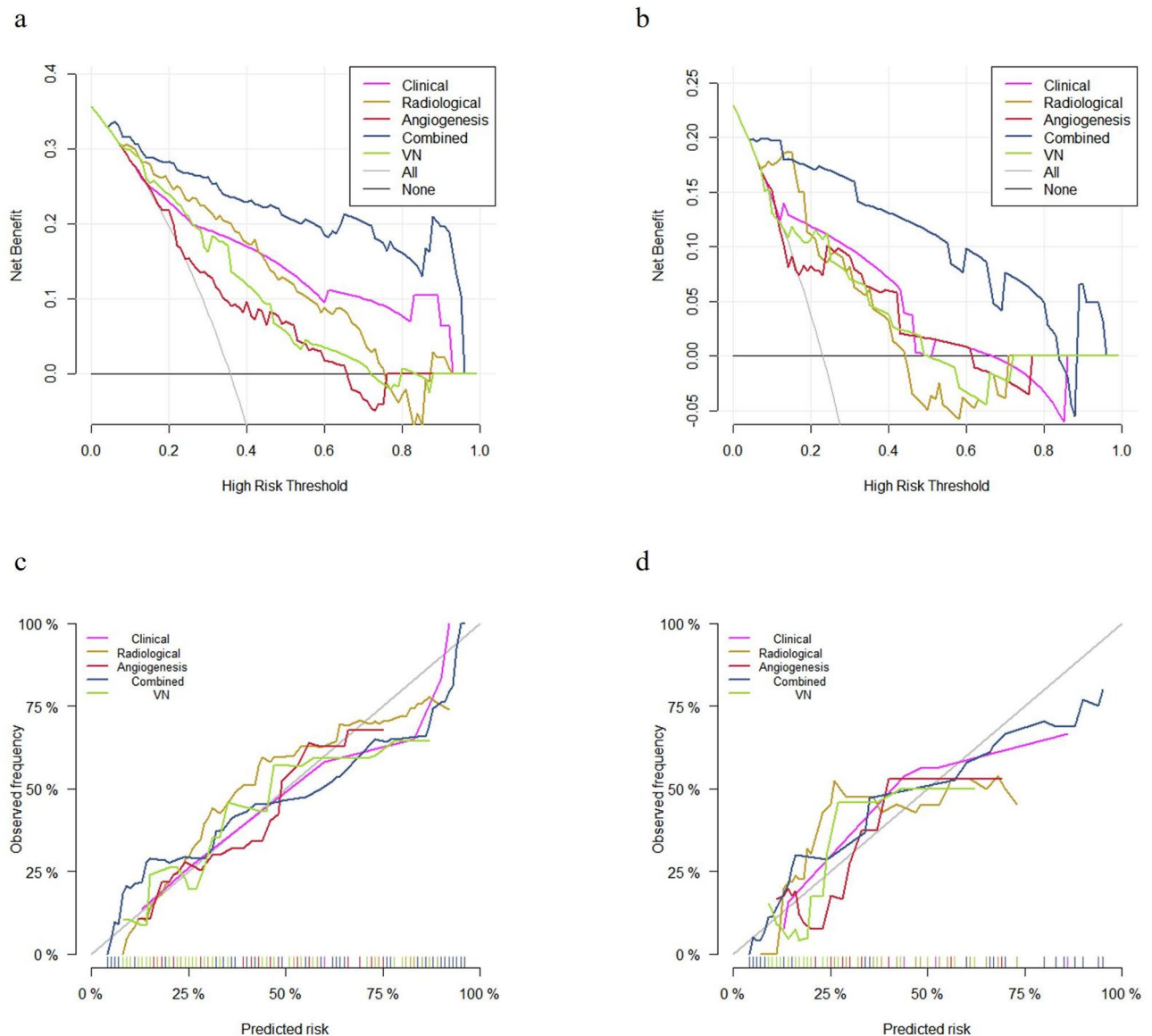
Fig. 4. Calibration curves and decision curves of different models. (**a**) Calibration curves in training cohort. (**b**) Calibration curves in validation cohort. (**c**) Decision curves in training cohort. (**d**) Decision curves in validation cohort.

Future impact

To translate the promising performance of the RACIM into routine clinical practice, prospective multicenter validation in diverse patient cohorts is essential. This will rigorously confirm its generalizability, stability across different SDCT platforms and operators, and real-world prognostic value. Integration into the clinical workflow could involve incorporating the RACIM score calculation into radiology reporting systems or hospital information systems (HIS/RIS/PACS) upon SDCT examination completion. The visualized risk stratification output could then be readily available within multidisciplinary team meetings, directly informing discussions on adjuvant therapy intensity (e.g., escalating or de-escalating chemotherapy) for individual LARC patients. Furthermore, exploring the development of automated or semi-automated tools for $NICVP_{3D}$ measurement within SDCT would enhance standardization, reduce observer variability, and facilitate the seamless adoption of this quantitative biomarker into future prospective studies and clinical practice, ultimately paving the way for its role in optimizing LARC treatment strategies.

Conclusion

The 3D-SDCT analysis protocol improved interobserver consistency, and the NICVP obtained by this method has the potential for predicting DFS. Moreover, our study highlighted the prognostic value of CD105-based MVD in rectal cancer. Furthermore, the multidimensional RACIM combined with SDCT, angiogenesis and clinicopathological parameters could offer an optional novel approach to improve the postoperative risk
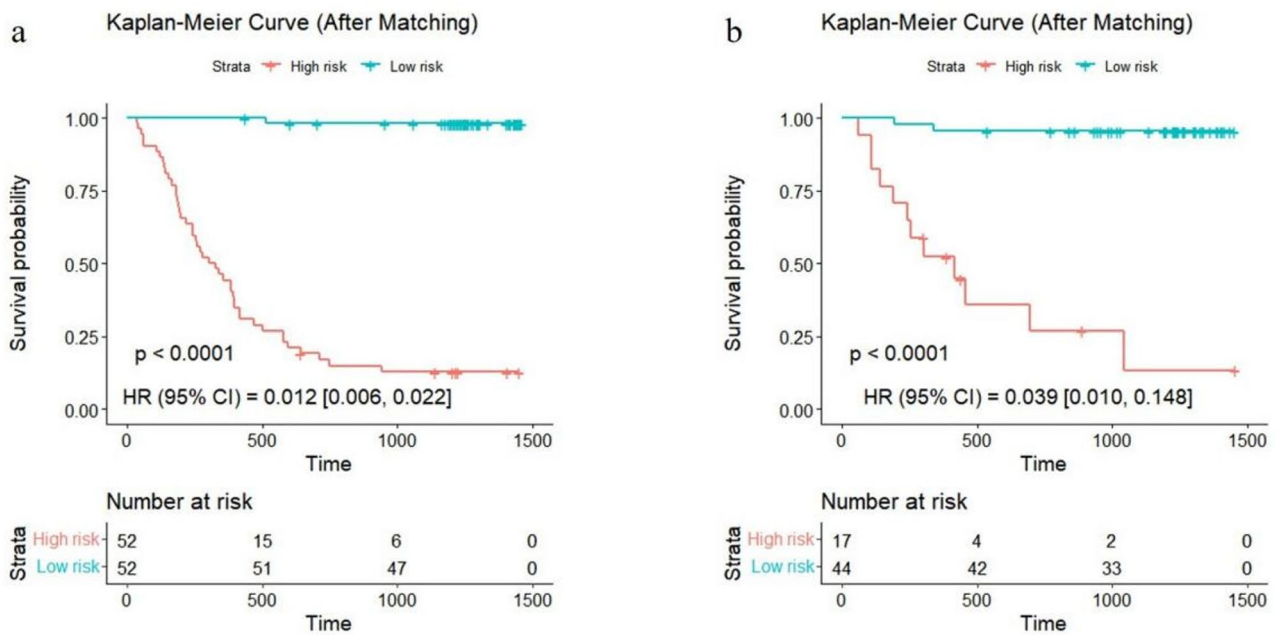
Fig. 5. The Kaplan Meier survival analysis curve stratified the prognosis of patients according to the RACIM-based classifier. (**a**) Training cohort. (**b**) Validation cohort.

	High-risk ($n = 69$)	Low-risk ($n = 135$)
$NICVP_{3D}$ (mean ± SD)	0.51 ± 0.09	0.35 ± 0.10
CD105(mean ± SD)	31.55 ± 5.67	26.57 ± 4.61
PNI, n (%)		
Absent	44(63.8%)	133(98.5%)
Present	25(36.2%)	2(1.5%)
HG, n (%)		
Well	20(29.0%)	75(55.6%)
Moderate	20(29.0%)	44(32.6%)
Poor	29(42.0%)	16(11.9%)

Table 5. Selected prediction parameters in RACIM-classified high and low-risk groups. NIC = normalized iodine concentration; VP = venous phase; PNI = perineural invasion; HG = histologic grade.

stratification in LARC patients. Our prediction model provided individual-level interpretability through the SHAP algorithm, providing a valuable decision-making basis for personalized postoperative therapeutic strategies.
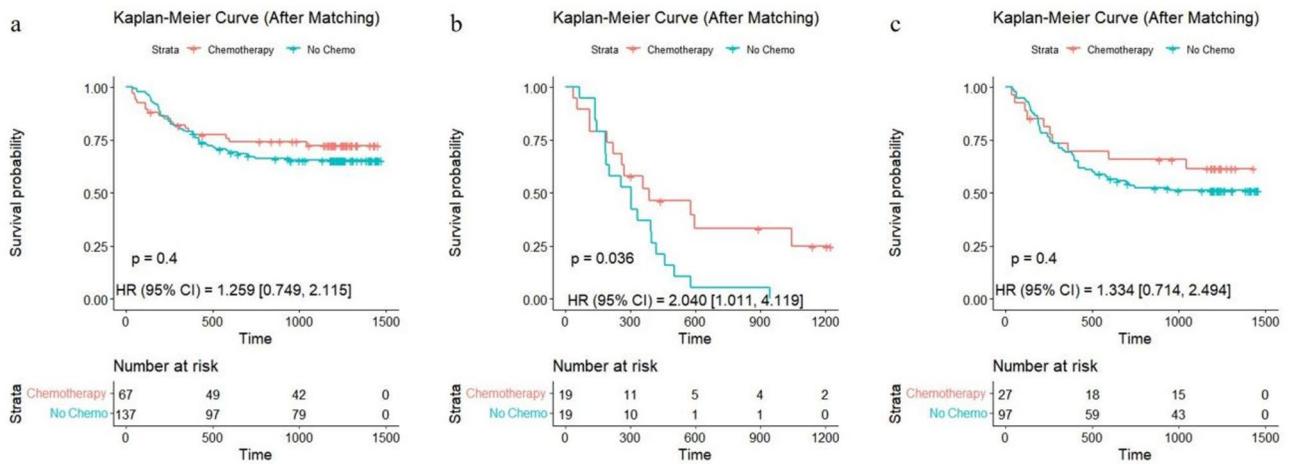
Fig. 6. Effect of postoperative adjuvant chemotherapy in different subgroups, which were stratified by the receipt of chemotherapy. (**a**) All cases group. (**b**) RACIM-classified high risk group. (**c**) Any high-risk clinicopathological features group.
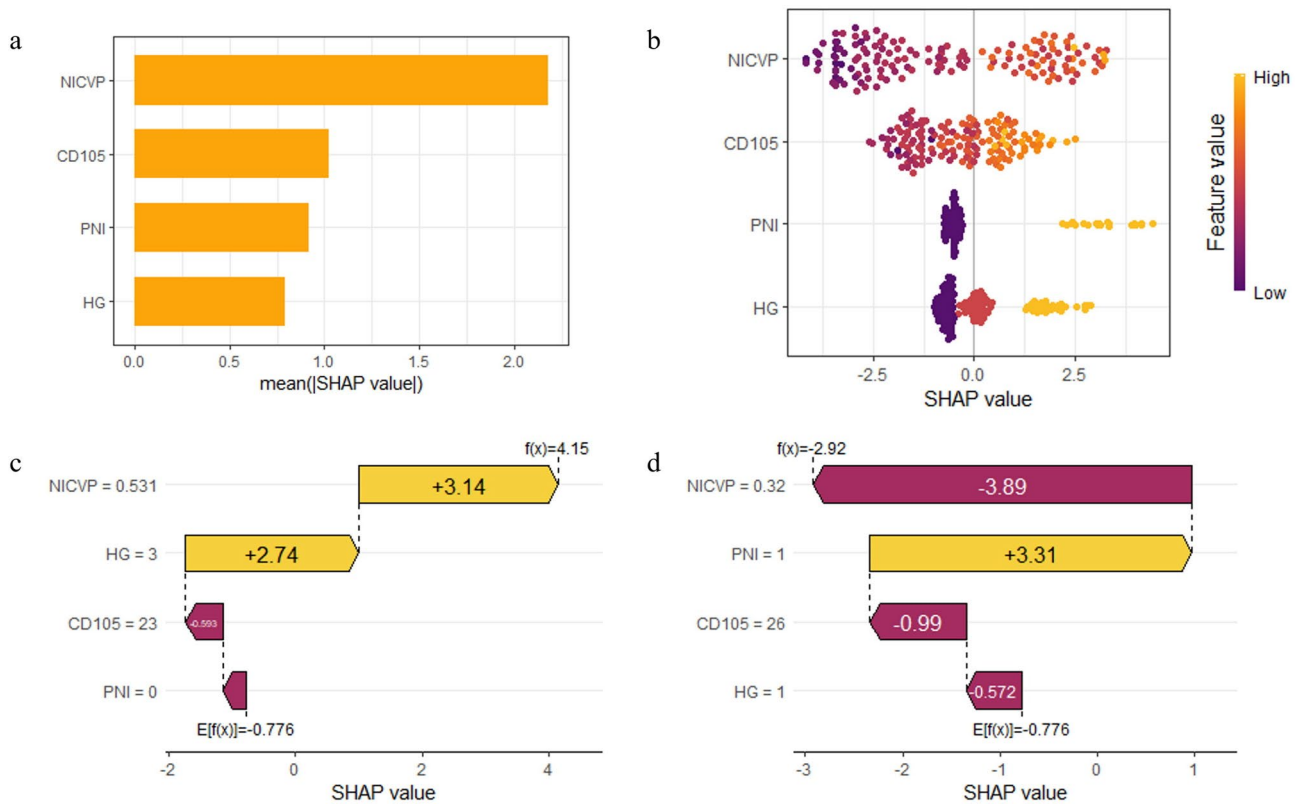
Fig. 7. Model interpretability of the RACIM for the prediction of disease-free survival (DFS) with SHAP in the training cohort. (**a**) Feature importance plot listing the most significant variables in descending order. (**b**) Summary plot of the impact of features on model decision-making and the interactions between features in the model. SHAP force plots of two participants with high (**c**) and low (**d**) risk of DFS. Yellow dots represent higher eigenvalues and purple dots represent lower eigenvalues.

Data availability
The data can be accessed upon request with a research proposal submitted to the investigator via the corresponding author.

References

1. Sebag-Montefiore, D. et al. Preoperative radiotherapy versus selective postoperative chemoradiotherapy in patients with rectal cancer (MRC CR07 and NCIC-CTG C016): a multicentre, randomised trial. *Lancet* **373**, 811–820 (2009).
2. Rödel, C. et al. Preoperative chemoradiotherapy and postoperative chemotherapy with fluorouracil and oxaliplatin versus fluorouracil alone in locally advanced rectal cancer: initial results of the German CAO/ARO/AIO-04 randomised phase 3 trial. *Lancet Oncol.* **13**, 679–687 (2012).
3. Breugom, A. J. et al. Adjuvant chemotherapy for rectal cancer patients treated with preoperative (chemo) radiotherapy and total mesorectal excision: a Dutch colorectal cancer group (DCCG) randomized phase III trial. *Ann. Oncol.* **26**, 696–701 (2015).
4. Fokas, E. et al. Tumor regression grading after preoperative chemoradiotherapy for locally advanced rectal carcinoma revisited: updated results of the CAO/ARO/AIO-94 trial. *J. Clin. Oncol.* **32**, 1554–1562 (2014).
5. National Comprehensive Cancer Network. NCCN Guidelines Rectal Cancer. National Comprehensive Cancer Network. (Version 6. 2023). (Accessed 23 December 2023). https://www.nccn.org/professionals/physician_gls/pdf/rectal.pdf.
6. Valentini, V. et al. Nomograms for predicting local recurrence, distant metastases, and overall survival for patients with locally advanced rectal cancer on the basis of European randomized clinical trials. *J. Clin. Oncol.* **29**, 3163–3172 (2011).
7. Amin, M. B. et al. The eighth edition AJCC cancer staging manual: continuing to build a Bridge from a population-based to a more personalizedapproach to cancer staging. *CA Cancer J. Clin.* **67**, 93–99 (2017).
8. Sargent, D. J., Andre, T. & Grothey, A. Futher evaluating the benefit of adjuvant chemotherapy for colon cancer. *J. Clin. Oncol.* **34**, 3711–3712 (2016).
9. Pahlman, L. A. et al. Should the benefit of adjuvant chemotherapy in colon cancer be re- evaluated? *J. Clin. Oncol.* **34**, 1297–1299 (2016).
10. Hwang, I. et al. Tumor-associated macrophage, angiogenesis and lymphangiogenesis markers predict prognosis of non-small cell lung cancer patients. *J. Transl Med.* **18**, 443 (2020).
11. Fox, S. B. Tumour angiogenesis and prognosis. *Histopathology* **30**, 294–301 (1997).
12. Zheng, S. et al. Identification of the angiogenesis related genes for predicting prognosis of patients with gastric cancer. *BMC Gastroenterol.* **21**, 146 (2021).
13. Parakh, A. et al. Dual-energy CT images: pearls and pitfalls. *Radiographics* **41**, 98–119 (2021).
14. Cao, Y. et al. Development of a dual-energy spectral computed tomography-based nomogram for the preoperative discrimination of histological grade in colorectal adenocarcinoma patients. *J. Gastrointest. Oncol.* **12**, 544–555 (2021).
15. Al-Najami, I., Lahaye, M. J., Beets-Tan, R. G. H. & Baatrup, G. Dual-energy CT can detect malignant lymph nodes in rectal cancer. *Eur. J. Radiol.* **90**, 81–88 (2017).
16. Al-Najami, I., Drue, H. C., Steele, R. & Baatrup, G. Dual energy CT-a possible new method to assess regression of rectal cancers after neoadjuvant treatment. *J. Surg. Oncol.* **116**, 984–988 (2017).
17. Wu, J. et al. The value of single-source dual-energy CT imaging for discriminating microsatellite instability from microsatellite stability human colorectal cancer. *Eur. Radiol.* **29**, 3782–3790 (2019).
18. Fan, S. X. et al. Correlations between the iodine concentrations from dual energy computed tomography and molecular markers Ki-67 and HIF-1α in rectal cancer: A preliminary study. *Eur. J. Radiol.* **96**, 109–114 (2017).
19. Hanahan, D. & Weinberg, R. A. Hallmarks of cancer: the next generation. *Cell* **144**, 646–674 (2011).
20. Abdalla, S. A. et al. Prognostic relevance of microvessel density in colorectal tumours. *Oncol. Rep.* **6**, 839–842 (1999).
21. Akagi, K. et al. Estimation of angiogenesis with anti-CD105 immunostaining in the process of colorectal cancer development. *Surgery* **131** (Suppl 1), S109–S113 (2002).
22. Nogués, A. et al. Endoglin (CD105) and VEGF as potential angiogenic and dissemination markers for colorectal cancer. *World J. Surg. Oncol.* **18**, 99 (2020).
23. Lundberg, S. M. & Lee, S. I. A unified approach to interpreting model predictions. In *Proceedings of the 31st international conference on neural information processing systems.* 4768-77. (Neural Information Processing Systems Foundation, Inc. (NIPS), 2017).
24. Li, J. et al. Spectral CT-based nomogram for preoperative prediction of perineural invasion in locally advanced gastric cancer: a prospective study. *Eur. Radiol.* **33**, 5172–5183 (2023).
25. Liang, P., Ren, X., Gao, J., Chen, K. & Xu, X. Iodine concentration in spectral CT: assessment of prognostic determinants in patients with gastric adenocarcinoma. *Am. J. Roentgenol.* **209**, 1033–1038 (2017).
26. Gao, W. et al. Association between extramural vascular invasion and iodine quantification using dual-energy computed tomography of rectal cancer: a preliminary study. *Eur. J. Radiol.* **158**, 110618 (2023).
27. Chen, X. H. et al. Spectral computed tomography in advanced gastric cancer: can iodine concentration non-invasively assess angiogenesis? *World J. Gastroenterol.* **23**, 1666–1675 (2017).
28. Pammar, C., Nayak, R. S., Kotrashetti, V. S. & Hosmani, J. Comparison of microvessel density using CD34 and CD105 in oral submucous fibrosis and its correlation with clinicopathological features: an immunohistochemical study. *J. Cancer Res. Ther.* **14**, 983–988 (2018).
29. Langer, E. M. et al. ZEB1-repressed MicroRNAs inhibit autocrine signaling that promotes vascular mimicry of breast cancer cells. *Oncogene* **37**, 1005–1019 (2018).
30. Fonsatti, E., Nicolay, H. J. M., Altomonte, M., Covre, A. & Maio, M. Targeting cancer vasculature via endoglin/CD105: a novel antibody-based diagnostic and therapeutic strategy in solid tumours. *Cardiovasc. Res.* **86**, 12–19 (2010).
31. Dallas, N. A. et al. Endoglin (CD105): A marker of tumor vasculature and potential target for therapy. *Clin. Cancer Res.* **14**, 1931–1937 (2008).

Author contributions

S.F., L.Q. and X.C. conceived and designed the study. S.F., J.L., X.Y., L.Q. acquired clinical data. S.F., L.X., L.Q., X.C. acquired and analyzed imaging data.S.F. performed the statistical analysis. S.F. and X.C. drafted the manuscript. All authors revised and amended critical parts of the manuscript. All authors contributed to the interpretation of the data and approved the final version of this manuscript.

Funding

Declarations

Competing interests
The authors declare no competing interests.

Additional information
Supplementary Information The online version contains supplementary material available at https://doi.org/10.1038/s41598-025-14851-x.

Correspondence and requests for materials should be addressed to X.C.

Reprints and permissions information is available at www.nature.com/reprints.

Publisher's note Springer Nature remains neutral with regard to jurisdictional claims in published maps and institutional affiliations.